Raman analysis of strained graphene grown on dewetted cobalt

Raman analysis of strained graphene grown on dewetted cobalt.

Federico Beccaria[1,2], Elisabetta Landini[1], Ettore Vittone[1], Giampiero Amato[2,3]*

[1] Department of Physics, and NIS Interdepartmental Center, University of Torino, via Pietro Giuria 1, 10125 Torino, Italy

[2] Nanoscience and Materials Division, INRIM, Strada delle Cacce 91, Torino, Italy

[3] Department of Science and Technological Innovation, University of Eastern Piedmont ‘‘A. Avogadro’’, Viale T. Michel 11, 1512 Alessandria, Italy

Abstract

Graphene grows onto cobalt by means of diffusion of carbon atoms during the isothermal stage of exposure to hydrocarbon precursor, followed by precipitation during cooling. This method, largely applied with nickel catalyst, is known to produce continuous, but not uniform, layers with the concurrent presence of mono- and poly-graphene areas. With the aid of Raman mapping of graphene still lying onto its catalyst, we are able to consider the possible origins for the observed distortions of the phonon modes with respect to the well-known picture of the monolayer material. Optical effects, doping, the presence of multilayered islands and strain are kept into account. It is shown that some observations can be interpreted in terms of the occurrence of isotropic strain with an uniaxial component superimposed at the metal discontinuities. Strain is proposed to originate from the difference between the thermal expansion coefficients of graphene and cobalt. The present paper shows that inhomogeneities in graphene grown onto calalysts with high C solubility is not always directly related to excess of precipitation. The observation of strain in as-grown graphene opens the possibility of tailoring the electronic density of states via strain engineering directly during growth.

* Giampiero Amato: Tel. +39 011 0437903; giampiero.amato@uniupo.it

1. Introduction

Since its experimental discovery in 2004[1], the interest of the scientific community for graphene resulted in numerous publications, both on its production[2,3] and applications[4]. Chemical Vapor Deposition (CVD) is one of the most used techniques, mainly on Cu[5] and Ni[6,7] substrates, whereas Co has not received the same attention[8]. While in Cu the graphene growth process is limited to the catalyst surface, it is well known that in Ni or Co the C solubility is ~2 order of magnitude higher than in Cu, leading to C diffusion into the catalyst during the isothermal exposure to the gas source, followed by the graphene growth by C precipitation in the following cooling stage[9].

The most relevant difference on the growth mechanism of graphene on Co and Ni, stems on the different heat of precipitation of C into the metal substrate, as highlighted in [10]. Actually, Hasebe *et al.*[11] reported about a value for the heat of precipitation Δ in Co about twice than in Ni at temperatures below its Curie Temperature (T_C=1121 °C), because of the magnetic contribution in the calculation of the enthalpy. Since the graphene growth is normally done around 1000 °C, a temperature lower than T_C(Co), but higher than T_C(Ni), the thermally activated law describing the C solubility (β):

$$\beta = \beta_0 \cdot exp\left[\frac{-\Delta}{k_B \cdot T}\right], \tag{1.1}$$

holds for both metals (k_B is the Boltzmann constant and T the absolute temperature), but with activation energy Δ about twice in the Co case. Considering that the crosspoint between the two curves occurs at T~950 °C, carbon precipitation during cooling in the Co case is higher than in Ni at T>950 °C, whereas the opposite occurs at T< 950 °C. This is somehow equivalent to a faster cooling rate. According to Baraton *et al.*[6], two distinct mechanisms can be considered for the graphene growth via C precipitation, the first at high temperature which leads to large crystalline domains with low defect density, the second at low temperature, which mainly provides nano-crystalline graphene. Then, due to the higher heat of precipitation, graphene should grow on Co mainly by means of the first mechanism, typical of the higher T range, with enhanced coverage and encouraging electrical performances, as recently reported[10].

In that study[10], graphene deposition was carried out on Co thin films (500 nm thick) deposited on SiO_2. Being the surface energy of the metal atoms at the grain boundaries unbalanced by the adhesion energy with the substrate, a valley is formed upon heating on the metal surface, which grows vertically

and laterally. The time required for this valley to reach the substrate is named incubation time; it is generally shorter at the boundaries involving 3 or more grains[12,13] and longer at linear boundaries between two grains. These different incubation times give rise to film discontinuities of nearly-circular shape in the first case and grooves but without the fragmentation of the film, in the second.. Discontinuities in the Co film some hundreds nanometers thick are sometimes observed in typical graphene depositions done at temperatures (T=1000°C) considerably lower than the Co melting temperature (about 1475°C) for times of the order of several minutes, probably because, due to the high C solubility, the melting temperature of the Co-C system is somewhat reduced[11].

In [10], we reported about full coverage of the graphene sheet, although the Co substrate presented nearly-circular discontinuities resulting from dewetting. On film discontinuities, suspended graphene was observed, whose formation was ascribed to the rapid precipitation of C onto the Co surface during the beginning of the cooling stage.

The investigation of the graphene quality grown on a discontinuous Co substrate can be effectively carried out by means of the Raman Spectroscopy employed directly onto the metal supported graphene layer, which is possible because of the almost absent luminescence of the substrate. This fact could prove decisive for the optimization of graphene growth onto Co, which seem promising in view of production of transfer-free electrical devices[14] or the mechanical strain-induced band gap engineering[15,16].

Many information can be extracted from Raman spectra of graphene by analyzing the three typical features arising at ~1598 cm^{-1} (the so-called G peak), ~2690 cm^{-1} (the 2D peak arising from interaction with 2 phonons at different Dirac cones) and the competitive D peak, observed at ~1350 cm^{-1} (related to the relaxation of momentum conservation rule at defect points).

Although the 2D line-shape and the 2D/G intensity ratio provide a good measure of the number of layers in the case of exfoliated or Cu-grown CVD graphene, departures from this situation have been reported for Ni-grown[17] and on Co-grown[10] CVD graphene, and generally ascribed to spatial variations of the thickness of the graphene layer. Apart from such spatial inhomogeneities, there are however other possible origins for the broadening/softening of the 2D mode, including optical effects, doping induced by the metal substrate, and strain, possibly originated by the different thermal expansion of graphene and its substrate.

In this work, Raman maps of graphene areas, directly taken on the discontinuous Co growth substrate, are analyzed, trying to uncouple the different contributions to the distortion of the Raman modes. It will be described how optical and doping effects can be easily recognized in the Raman spectra, whereas more complicated analyses are required in the cases of strain and the presence of multilayered regions.

2. Experimental

Graphene was synthesized via Rapid Cooling CVD, as proposed in [10], using a Rapid Thermal Annealing (RTA) apparatus[18]. The substrate and catalyst of choice was Co polycrystalline thin film, 500 nm thick, deposited by Radio Frequency (RF) Sputtering onto Si substrates with 500 nm thermal SiO_2. Prior to the graphene deposition, the Co/SiO_2 substrate was cleaned in sonic bath with acetone and ethanol. The deposition temperature of 1000 °C was reached with a rate of ~2.5 °C/s. In the isothermal stage, the first 5 minutes consisted in the reduction of the native Co oxide in Ar (50 SCCM) and H_2 (30 SCCM) atmosphere, followed by 5 min of deposition with 10 SCCM of CH_4 and 20 SCCM of H_2. The deposition was carried out a constant pressure of 670 Pa. The cooling stage, critical for CVD on Co[10] (as well as reported in [6] for Ni), was carried out in two steps: from 1000°C to 600°C at a rate of ~3.5 °C/s in Ar and H_2 atmosphere, and from 600°C to room temperature at the same rate under a 200 SCCM N_2 flux[2]. Fig. 1 summarizes the whole deposition process.

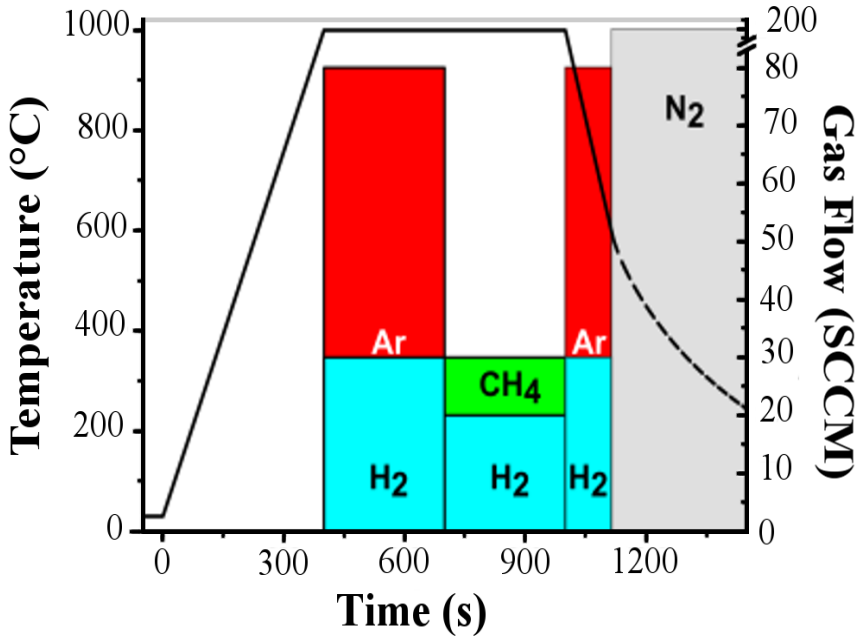

Fig. 1: Process flow with time of injected gases (stacked-area plot, right scale) and furnace temperature (continuous line, left scale).

Parts of the graphene samples were transferred to SiO_2 (316 nm)/Si substrates by means of a standard wet etching technique, as described in [10], and analyzed using a portable BWTEK model BWS415 Macro-Raman spectrometer, with a spot diameter of 100 μm and power density $\Psi \approx 150$ W/cm^2.

The direct micro-analysis of graphene on Co, was carried out by a home-made Scanning micro-Raman spectroscope[19], equipped with Diode Pumped Solid State Laser operating at a wavelength of λ=532 nm, focused to a spot diameter of 1 μm.

The Raman analysis was performed on spectra collected using a laser power density $\Psi \approx 2.54 \times 10^5$ W/cm^2, acquisition time t_{acq} = 60 s, resulting from the averaging of 2 acquisitions.

The same micro-Raman optics has been modified to perform reflectance measurements, focusing a white light beam on the sample; the reflectance spectra were acquired through an Ocean Optics USB4000 spectrometer

3. Results and Discussion

Fig. 2a shows a SEM image of the sample under study, after the graphene growth. Noticeably, in Fig. 2b, it is apparent the coverage of the hole with a graphene sheet. The graphene growth onto Co holes has been previously evidenced in [10], and interpreted in term of the concurrent surface precipitation of C and Co hole expansion during the cooling stage of the CVD process.

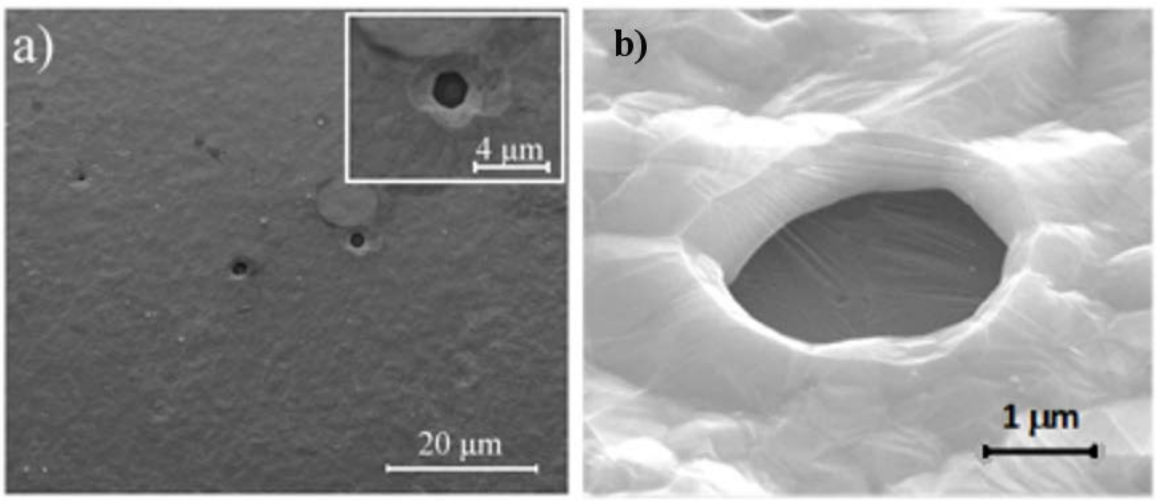

Fig. 2: a) low magnification SEM image of the sample evidencing the presence of holes formed during the graphene deposition process (Inset: Zoom on the hole region, b) high magnification SEM image of a hole covered with a graphene suspended membrane showing corrugations (discussed in the following).

A further confirmation of the continuity of the graphene film, in spite of the discontinuities in the catalyst beneath, is given by the Macro-Raman analysis on an area of about 8000 μm^2, on graphene transferred on SiO_2/Si substrate. Actually, the Raman spectrum in Fig. 3 shows that the D peak intensity is close to the detection limit of the instrument and the 2D/G ratio is about 4. Then, while the presence of multilayered regions due to excess of C precipitation cannot be excluded, relatively large sample

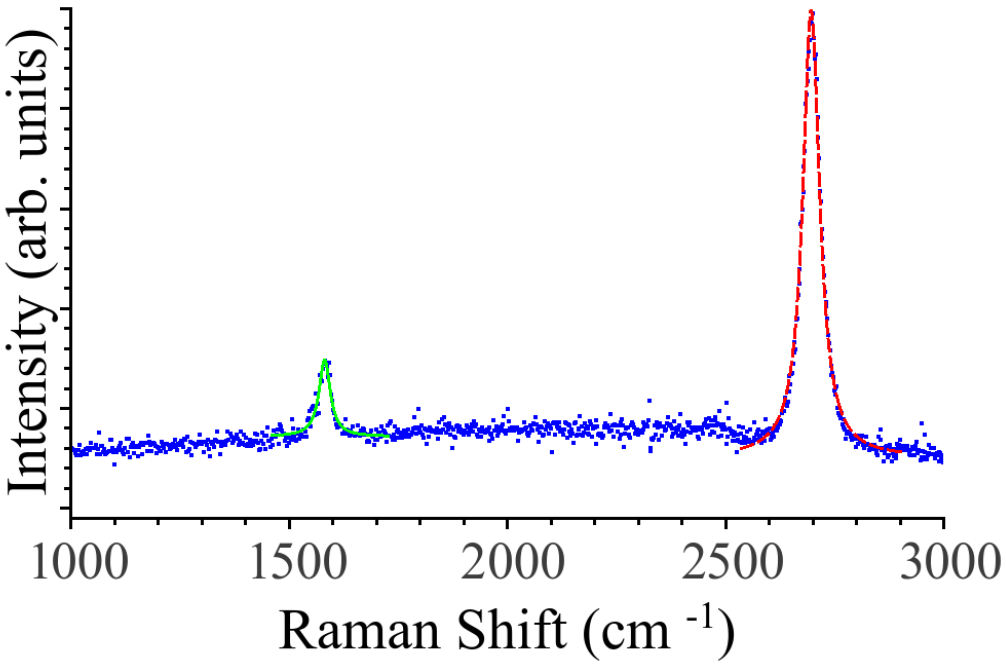

Fig. 3: Raman spectrum of graphene transferred onto SiO_2/Si, as collected with the BWTEK, model BWS415 Macro-Raman spectrometer. The dashed and solid lines are the lorentzian fits of the experimental data, relevant to the G and 2D modes, respectively.

areas with monolayer character can be found.

A more detailed investigation of the graphene features on dewetted Co requires an accurate Raman analysis directly on the growth substrate, which is here allowed because Raman spectra from graphene deposited on a Co substrate, differently from Cu[20], are not affected by a broad photoluminescence background, if generated by a green laser beam[21].

Fig. 4 (a, b) shows G and D intensity maps of a (20x20) μm^2 region of graphene on Co, respectively. It is apparent in both the maps, the presence of five high intensity regions, which we attribute to graphene grown onto five holes of the Co substrate. This analysis allows us to investigate the effect of

the substrate discontinuities on both the enhancement of the optical Raman emission and the structure of the graphene above and around the holes.

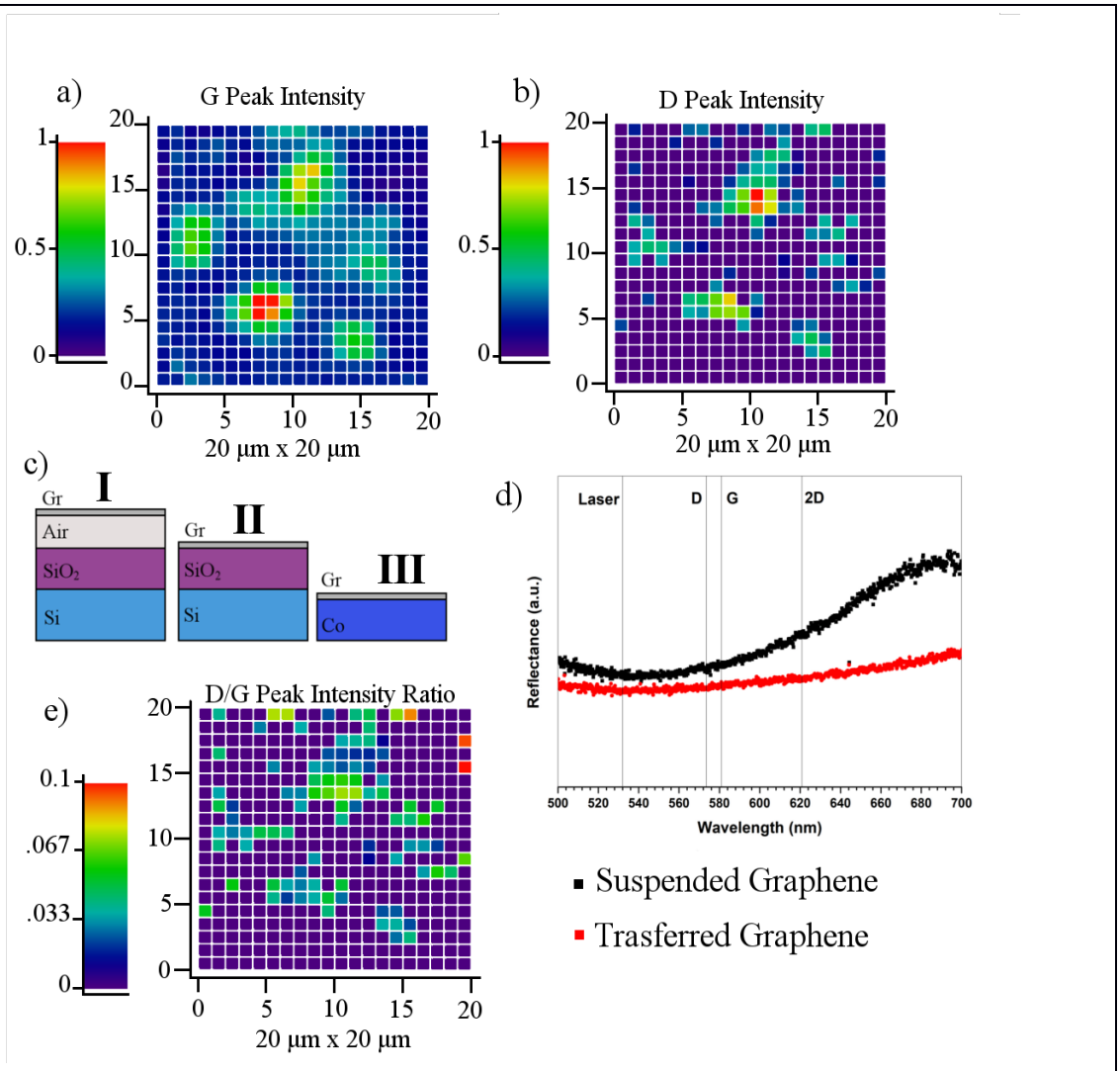

Fig. 4. Raman maps, normalized to the maximum intensity, of the G a) and D b) modes. c) Scheme of the graphene grown on holes (I), transferred on SiO_2 (II), grown on Co (III). d) Reflectance curves of suspended and transferred graphene. Vertical lines indicate the wavelengths of the laser excitation line and the Raman modes under study. The curve of graphene on Co has been omitted, being the reflectance very low and almost constant in the investigated wavelength range. e) Raman map of the D/G intensity ratio.

Actually, the amplification of the Raman signals can be ascribed to interference effects[22,23], occurring for the structure Graphene/Air (500 nm)/SiO_2 (500 nm)/Si (see Fig. 4c-I); here the 500 nm air layer takes the place of the 500 nm Co film removed by dewetting. The optical path of the laser beam in the air layer is similar to the common Graphene/SiO_2 (~300 nm)/Si assembly (see Fig. 4c-II), whereas no interference occurs in the Graphene/Co structure (see Fig. 4c-III).

This interpretation is corroborated by the related reflectance spectra shown in Fig. 4d, which evidence that the reflectance curve of the structure in 4c-I is similar to that of the structure in 4c-II at the wavelengths relevant to the laser excitation and to the D and G Raman modes.

Since the difference in wavelength of the G and D modes is ~8 nm, the high intensity of the D peak on the holes cannot be ascribed to a real increase of defects on the region, rather to a simple optical amplification due to multiple reflections in the graphene/air/SiO_2/Si structure. The intensity ratio D/G, shown in Fig. 4e, displays a rather uniform spatial distribution of defects in the investigated area, not exceeding 10%, and with an average value of 0.97%, fully compatible with the Macro Raman investigation carried out on the graphene transferred onto the SiO_2/Si structure.

Noticeably, in the investigated area, we observe a remarkable increase of the D/G ratio only for one of the five holes in the Co substrate (centred at coordinate (10,13)). This can be interpreted as the presence of discontinuities of the graphene layer itself, nevertheless no clear evidence of graphene disruptions is observed onto the remaining holes.

A similar analysis was carried out for the 2D feature. Fig. 5 a) and b) display the 2D normalized intensity and 2D/G ratio maps, respectively, onto the five holes under investigation. Results indicate spectral signatures of multilayered graphene on the holes; specifically the 2D/G intensity ratio is about 0.8. However, as previously mentioned, the interference effect on the holes plays an important role enhancing the Raman signals, but differently from the D/G case, here a great care must be applied, since the difference in wavelengths between the 2D and G peaks is 40 nm, which could lead to a very different interference behaviour[22].

Calculations of the enhancement factor, as described by Yoon *et al.*[22] have been performed by means of the Rouard recursive algorithm[24], for three different optical systems, namely Graphene/Air (500 nm) /SiO_2 (500 nm) /Si, Graphene/Co (500 nm) and Graphene/SiO_2 (316 nm)/ Si, as shown in Fig. 6 (see Appendix).

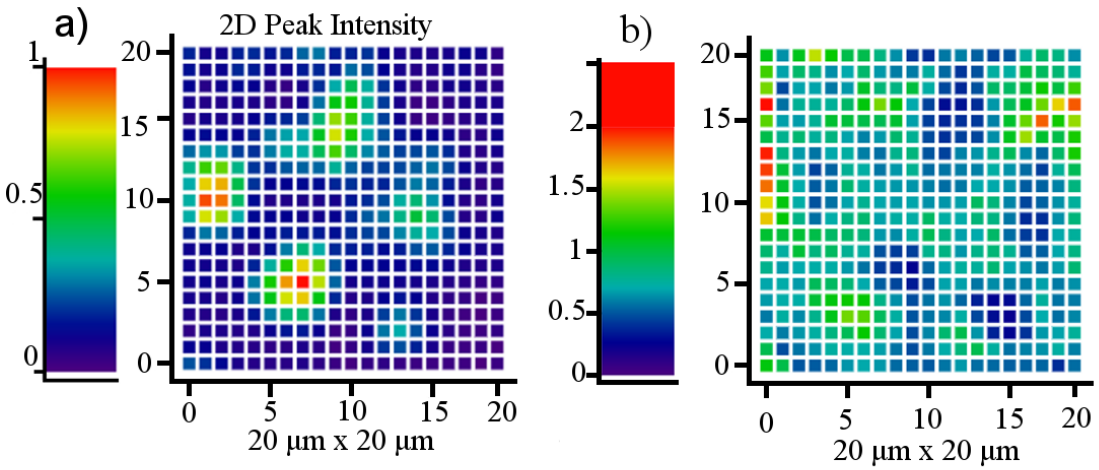

Fig. 5 a) Raman map of the 2D mode, b) the 2D/G intensity ratio obtained by combining data in a) (2D mode) and in Fig. 4a (G mode).

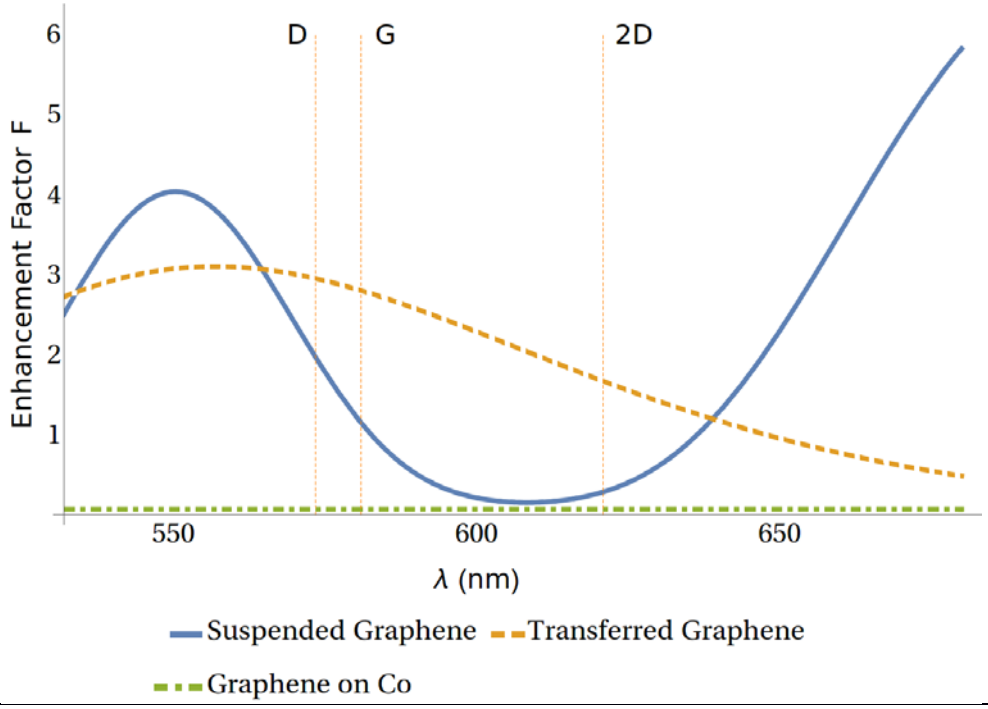

Fig. 6 The calculated enhancement factor for Raman modes under 532 nm excitation, for the three different optical assemblies under study.

The ratio of the enhancement factor relevant to the 2D and G peaks for the Graphene/Air/SiO_2/Si assembly is $(F_{2D}/F_G)_I$=0.285/1.150=0.248, whereas for Graphene/SiO_2/Si assembly is $(F_{2D}/F_G)_{II}$=1.668/2.799=0.596. This means that the 2D/G intensity ratio of graphene on the hole is about 40% than the 2D/G intensity ratio of graphene lying onto SiO_2. Therefore, the average value of 0.8 of the 2D/G intensity ratio of graphene on the holes shown in Fig. 5b, corresponds to a value of about 2 if referenced to the more conventional case of graphene on SiO_2, which is widely considered in literature as a typical signature for the presence of monolayer graphene[25]. In a similar way, we can correct the 2D/G intensity ratio evaluated on Co by noting that the enhancement factor is constant in that case. Then, to compare with the Graphene/SiO_2/Si assembly it is enough to multiply by $(F_{2D}/F_G)_{II}$=0.596, obtaining a 2D/G ratio of the order of 0.5. Then, excess of C precipitation takes place in the regions surrounding Co holes. Such result confirms the widely accepted explanation that C excess occurs in Ni and Co preferentially at the curved regions of the metal surface, mainly at grain boundaries[5], due to the composition of vertical and horizontal precipitation[6]. Then, the vertical mechanism is inhibited on Co holes, and monolayer graphene is formed. Growth is then expected to be inhomogeneous in “holey” Co areas, with a large variation from mono- to multi-layer.

The Full Width Half Maximum (FWHM) of the Raman features is another useful parameter to determine the properties of the graphene layer. In particular, we observed broadening and shifting of the 2D peak. Actually, Fig. 7 shows typical shapes of the 2D peak, relevant to regions on the hole and on Co, and compared with the 2D peak acquired onto a graphene layer, grown on Cu foil and transferred on SiO_2/Si, and considered as a reference sample. Both spectra relevant to graphene grown on Co can be fitted with two Lorentzian line-shapes, named $2D^+$ and $2D^-$, hereafter. Convolution of different modes is a typical feature of bi- and multi-layered graphene, but this commonly used interpretation seems not compatible with the previous observation of the monolayer nature of graphene grown on holes. As displayed in Fig. 2b, the suspended graphene membrane shows corrugations as possible effect of a strain component directed in parallel. By cutting the monolayer graphene membrane orthogonal to corrugations by means of a Quanta 3D Focused Ion Beam (FIB), those disappear indicating that strain has relaxed (Fig. 8). The broadened shape of the cut is a further confirm for this explanation. Then it can be inferred that the 2D splitting in the suspended monolayers originates from strain.

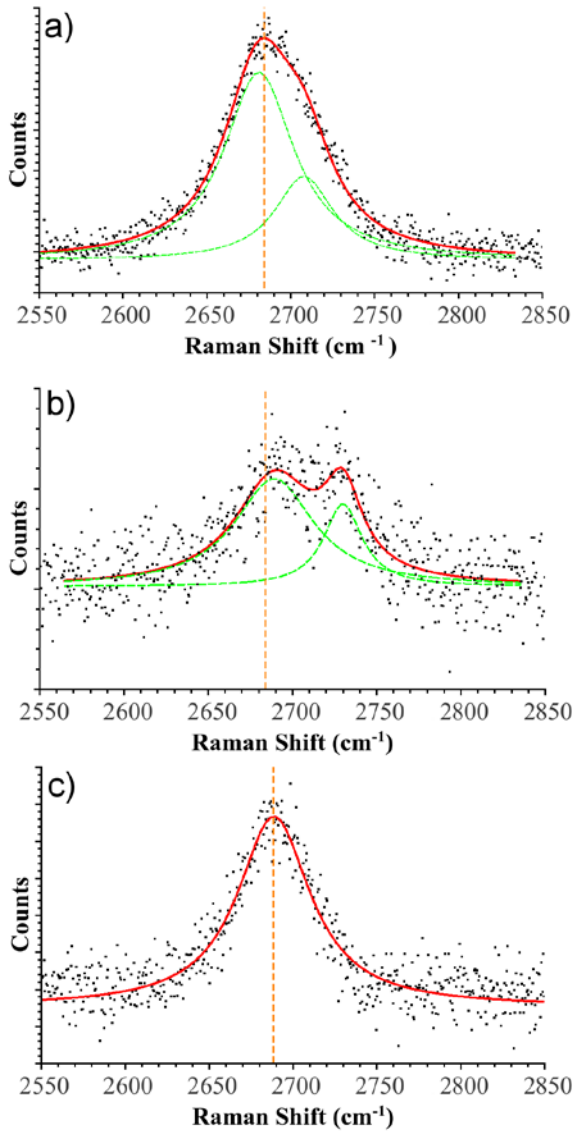

Fig. 7: 2D Raman spectra relevant to: a) graphene grown on a hole of the Co substrate, b) graphene grown on the Co substrate; c) graphene grown on Cu foil and transferred on SiO_2/Si, considered as a reference sample. The full lines are the convolution of the two fitting Lorentzian dashed curves. The vertical line identifies the 2D peak centroid position for the graphene reference sample in c).

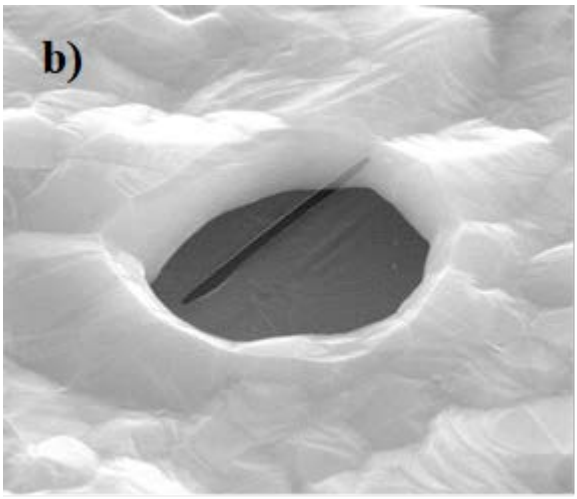

Fig. 8. SEM micrograph of the same graphene membrane depicted in Fig. 2b after cutting with a Focused Ion Beam. The elliptical shape of the cutting, together with the disappearance of the corrugations orthogonal to the cut prove that strain has relaxed.

The situation is well displayed in Fig. 9 relevant to a region where one hole can be easily localized in the 2D peak intensity map (Fig. 9a), by virtue of the aforementioned enhancement optical effect. Correspondingly, the map in Fig. 9b of the variable $\xi = (2D^+ + 2D^-)/2$, which represents the shift of the centroids of the two Lorentzian components $2D^+$ and $2D^-$, and the map in 9c) relevant to the splitting $\delta = (2D^+ - 2D^-)$, shows complementary aspects. It is worth noticing that the centroid must not be confused with the center-of-mass of the full feature, because it does not depend on the relative intensities of the two components. Extending the analysis to the region surrounding the hole, where graphene adheres to Co, we observe that, in spite of a relative uniform intensity of the 2D peak (Fig. 9a), its centroid position and splitting varies in a noticeable fashion along the investigated area.

The scatter plot of δ vs. ξ shown in Fig. 10a seems to be compatible with an interpretation, commonly adopted in materials deposited onto similar catalysts (Ni[6,7]), based on the inhomogeneity due to the presence of regions with a different number of layers[14,25,26]. In particular, the evidence that many points suffer a 2D blue-shift, would seems to support this interpretation. However, if that is the case, an intense D peak should be expected–at the borders of the terracing, that, on the contrary, has been described above to be negligible on the macroscopic analysis (Fig. 3) of transferred graphene just occurring in very small areas, as visible in Fig. 4e. We can conclude, with the additional support from the constancy

of the 2D peak (the green half spot on the right side of the map in Fig. 9a is due to another hole), that the graphene sheet lying on Co is relatively uniform, no matter if mono- , bi- or multi-layer

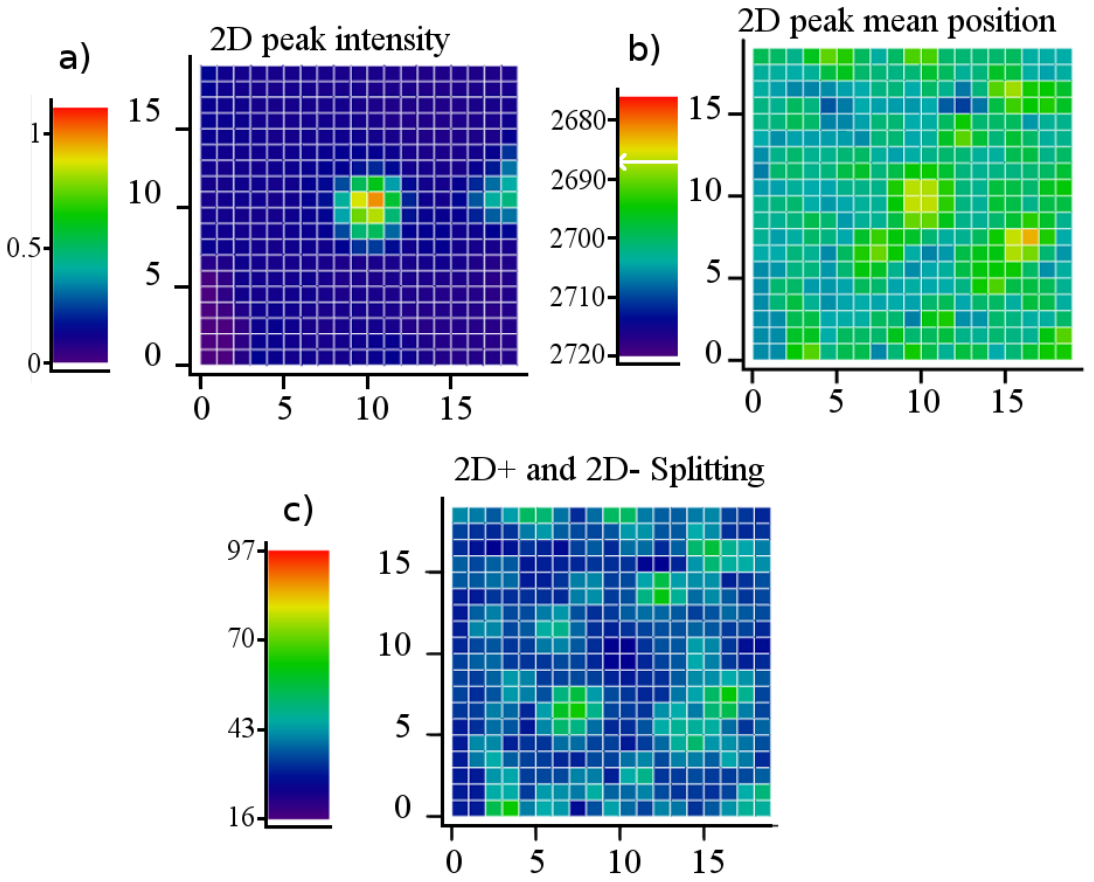

Fig. 9: a) Intensity map of the 2D peak; b) position map of the 2D centroid $\xi=(2D^{+}+2D^{-})/2$; c) map of the difference $\delta=2D^{+}-2D^{-}$between the centroids of the two Lorentzian curves.

At a closer look of the scatter plot in Fig. 10a, there is a non-negligible fraction (including the hole whose points pertain to the D region) of the investigated area showing a red-shift of the 2D peak. We observed that especially on the material lying on Co, red-shift is accompanied with a large splitting (circle B), whereas when the blue-shift occurs, splitting is reduced (circle C). This observation is not compatible with the usual model of the 2D shape as a function of the number of layers[25]. Here, on the contrary (see Fig. 10a), it seems that δ depends on ξ in a linear way, with negative angular coefficient,

and with the two components of the 2D feature collapsing around 2730 cm^{-1}. This observation leads to rule out the interpretation which assumes the material as structured in a mosaic of graphene multilayers.

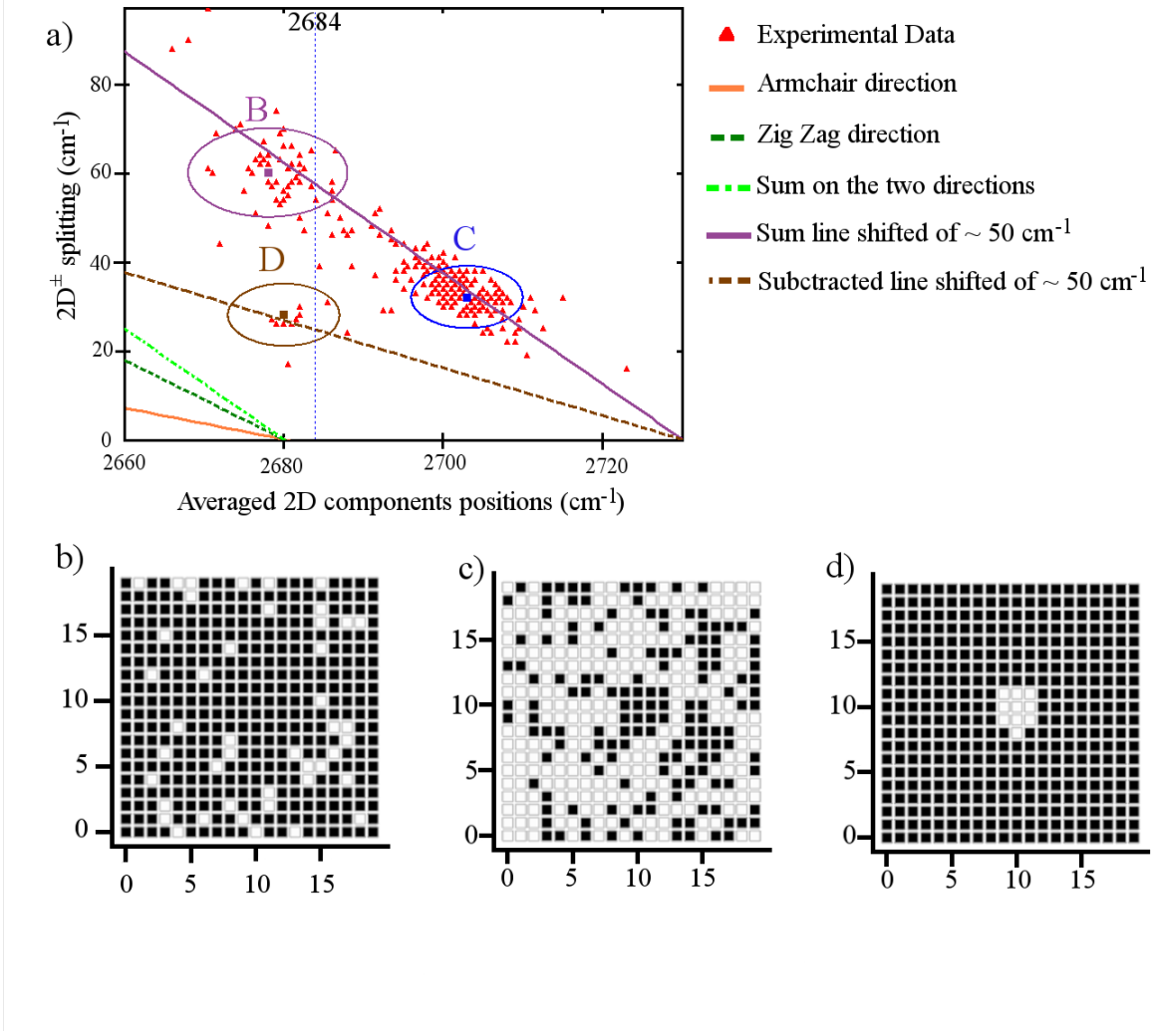

Fig. 10: a) scatter plot of δ vs. ξ. The circled areas B, C, and D are correlated to the white spots in the maps b), c) and d). The dashed vertical line indicates the centroid of the transferred (unstressed) graphene. The lines in the bottom-left corner of panel a) represent the linear relationships between δ and ξ taken from[28] for the armchair (full) and zig-zag (dashes) directions, respectively. The dashed-dotted line is the sum of those two straight lines. The full line crossing the circles B and C is parallel to the latter and shifted of 50 cm^{-1}. The dashed line crossing circle D is the difference of these two straight lines shifted of 50 cm^{-1}, too.

Similarly, doping can hardly be interpreted as the solely cause of the data distribution in Fig. 10a. According to Das *et al.*[27], Co behaves as an electron donor for graphene and the relevant charge doping induces a red-shift of the 2D peak, which should permeate the whole area under study. However, only few, randomly distributed points showing 2D red shift are shown in Fig. 10b, whereas maps in Fig. 10c show a more uniform distribution of points with 2D blue shift.

An alternative interpretation is based on the effect of stress on graphene. Actually, Yoon *et al.*[28] reported about experimental data of uniaxial strain along armchair (A) and zig-zag (Z) directions, with linear dependence of Raman frequencies with the strain percent. Their analysis can be combined resulting in a straight-line dependence of the δ vs. ξ with a slope of $\partial\delta/\partial\xi = 0.35$ and 0.88 for the Z and A case, respectively; both the components collapse at $\xi = 2680$ cm^{-1}, as expected for the unstrained material. The continuous lines in the left bottom corner of Fig. 10a show these linear dependences. In our case a linear fit carried out on data relevant to graphene areas lying onto Co solely (i.e. excluding the suspended areas identified by the region D in Fig. 10a) yields a slope of -1.25 and an intercept of 2730 cm^{-1}.

Concerning the difference in the intercept with respect to the case of Yoon *et al.*[28], first we have to remark that the absence of any splitting does not necessarily imply absence of strain, but can arise from a more general case of hydrostatic strain, which is in principle able to provoke the same variation of all bonds length. Moreover, at the intercept, the energy is higher than the unstrained case, indicating the presence of isotropic compressive strain of graphene on Co. This agrees well with the belief that wrinkles are formed during cooling down due to the large difference of thermal expansion coefficient, reported to be negative in graphene[29–31]. In the real case, such background compressive strain composes with an uniaxial tensile component that originates likely from the retraction of Co crystallized during dewetting, and becomes dominant in some regions, displayed in Fig. 10b, giving rise to the red shift of ξ. This scenario results in a distribution of the data gathering around a straight line shown in Fig. 10a.

The interpretation based on strain effects is further corroborated by noticing that the sum of the two slopes from *Yoon et al.*[28] well agrees with the slope of the linear fit of our experimental data. Actually, the combination of a compressive and tensile strain in two orthogonal directions yields to an increase of the splitting, which is inherent to anisotropic changes of phonon branches with distorted Dirac cones,

and to a global reduction of ξ, which is relevant to the average bond strength compared to the unstrained case.

Based on this interpretation the meaning of data points lying in the circlet D of Fig. 10a, which corresponds to graphene grown on the hole (see Fig. 10d), is then evident. Here, a red-shift occurs together with a relatively small splitting, from which it can be argued that an almost isotropic tensile strain occurs, as expected for a graphene layer suspended onto a roughly circular discontinuity of the substrate radially expanding during cooling[10]. The relatively small splitting can then be attributed to the presence of radial tensile stress, which induces different strains along the two principal directions[28].

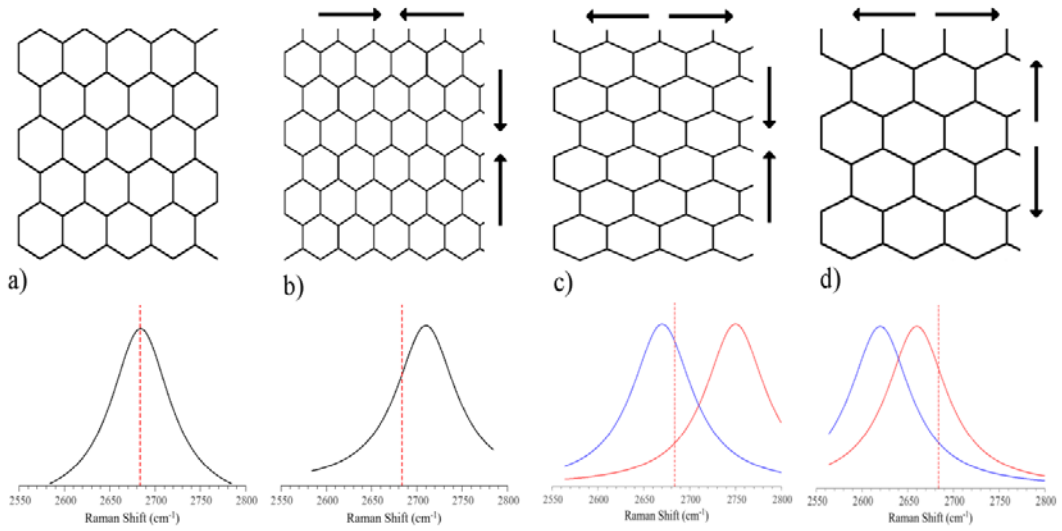

Fig. 11: Schematics of the graphene lattice and the 2D+ and 2D- components in the unstrained case (a), hydrostatic compressive strain (b), composition of orthogonal tensile and compressive strains (c) and composition of two orthogonal non equal tensile strains (d). Strains have been exaggerated for clarity.

Fig. 11 schematizes the effect of biaxial strain on the graphene lattice, and proposes an interpretation of the $2D^+$ and $2D^-$ components, according to the strain nature. Fig. 11a shows the unstrained case showing a unique peak; Fig. 11b displays the sample subjected to a hydrostatic compressive strain, resulting in an apparent blue-shifted 2D peak, with a negligible splitting of the $2D^+$ and $2D^-$ components. Fig. 11c

represents a biaxial strained sample, with tensile strain in the zigzag direction, whereas the strain in the armchair direction is compressive.

The resulting 2D peak can be decomposed in two contributions, with higher and lower Raman shift with respect to the unstrained case. Differently from above, as described in Fig. 11d, the two orthogonal equal stress components along A and Z directions correspond to slightly different strain components, because of the different Young moduli along A and Z. In other words, splitting in this case is the results of subtracting the two lines extracted by from Yoon *et al.*[28] and displayed in Fig. 10a. The fact that data points pertaining to the cloud D in Fig. 10a, which correspond to the suspended membrane, lie onto a straight line with intercept ξ=2730 cm^{-1} and slope 0.53, fits well into this scenario.

Strain can arise during cooling because of the thermal mismatch between substrate and graphene. Our results suggest that it is more intense in graphene grown on Co rather than in Ni though the thermal expansion coefficients Λ differ only by few percent (Λ_{Co}=1.3 10^{-5} K^{-1} and Λ_{Ni}=1.34 10^{-5} K^{-1})[32]. The more likely explanation suggests that the graphene layer is formed on Co at higher temperature, as a consequence for the heat of precipitation of C, twice in Co than in Ni[10]. Graphene grown in this way undergoes larger thermal mismatch compared to the Co metallic substrate, as a consequence of the larger temperature variation[33]. The resulting strain is then higher in the Co case.

4. Conclusions

In conclusion, analysis of Raman maps evidences a well-defined dependence of the splitting vs. shift of the 2D mode that can be hardly explained in terms of structural inhomogeneity's, say, presence of multilayered islands, or by n-type doping induced by the underlying substrate. On the contrary, a faithful description of the experimental observations is achieved by considering a background isotropic compressive strain, probably originating from volume compression of the metal during cooling, together with uniaxial tensile components at the grooves in correspondence of the grain boundaries of the metal. In deeper elliptical/circular metal discontinuities, on the other hand, the favorable optical structure allows to detect a small value of the 2D splitting, which is proposed to originate from different elastic responses along armchair and zigzag directions to the isotropic tensile stress.

Acknowledgments

One of the authors (F.B.) gratefully acknowledges the Istituto Nazionale di Ricerca Metrologica (INRiM) for the financial support through the "Nanotechnologies for Electromagnetic Metrology" program.

5. Appendix

5.1 Reflectance measurements simulation

The Rouard algorithm[24] for a stacked optical system, schematized in Fig. 4C and taking the Air/graphene/Air/SiO_2/Si system for completion (labelled 1/2/3/4/5 for simplicity), starts considering perpendicular reflection ($\theta = 0$) and the layer 4, with refraction index n_4, thickness e_4 and Fresnel reflective index $r_{4\text{-}5}$ as following:

$$r_{4-5} = \frac{n_4 cos(\theta) - n_5 cos(\theta)}{n_4 cos(\theta) + n_5 cos(\theta)} = \frac{n_4 - n_5}{n_4 + n_5}. \quad (5.1.1)$$

The Layer 4 is placed between layer 3 and layer 5, and the light transmission into the material induces a phase change φ_k:

$$\varphi_k = \frac{2\pi}{\lambda} n_k e_k cos(\theta_k) = \frac{2\pi}{\lambda} n_k e_k. \quad (5.1.2)$$

The phase change is introduced in the calculation of the Fresnel effective reflective index of layer 4 as:

$$r_4 = \frac{r_{3-4} + r_{4-5} e^{-2i\varphi_4}}{1 + r_{3-4} r_{4-5} e^{-2i\varphi_4}}. \quad (5.1.3)$$

Proceeding upwards layer-by-layer with the algorithm, the Fresnel refractive index of the system can be calculated. The complex refractive indexes for SiO_2, Si, graphene and Co have been considered as constant (1.46; 4.15 + 0.052 *i*; 2.6 + 1.3 *i*; 2 + 3.74 *i* respectively[34])

5.2 Enhancement factor calculation

The enhancement factor formulation given by Yoon *et al.*[22] has been constructed considering multiple interactions of the scattered laser light with the layer of graphene. The authors consider two terms for the calculation, namely an absorption term F_{ab} and a scattering term F_{sc}:

$$F_{ab} = t_1 \frac{\left[1+r_{2-3}r_4e^{-2i\varphi_3}\right]e^{-i\varphi_x}+\left[r_{2-3}+r_4e^{-2i\varphi_3}\right]e^{-i(2\varphi_2-\varphi_x)}}{1+r_{2-3}r_4e^{-2i\varphi_3}+\left(r_{2-3}+r_4e^{-2i\varphi_3}\right)r_{1-2}e^{-2i\varphi_2}} \tag{5.2.1}$$

$$F_{sc} = t'_1 \frac{\left[1+r_{2-3}r_4e^{-2i\varphi_3}\right]e^{-i\varphi_x}+\left[r_{2-3}+r_4e^{-2i\varphi_3}\right]e^{-i(2\varphi_2-\varphi_x)}}{1+r_{2-3}r_4e^{-2i\varphi_3}+\left(r_{2-3}+r_4e^{-2i\varphi_3}\right)r_{1-2}e^{-2i\varphi_2}}, \tag{5.2.2}$$

where t_i and r_i are the Fresnel transmittance and reflection coefficients and φ_i are the phase changes as defined in the previous section. In particular, t_1 and t'_1 are defined as:

$$t_1 = \frac{2n_1}{n_1+n_2}\ , \quad t'_1 = \frac{2n_2}{n_2+n_1}, \tag{5.2.3}$$

and φ_x is defined with a spatial variable x, which is the point where the Raman interaction occurs.

$$\varphi_x = \frac{2\pi}{\lambda} n_2 x. \tag{5.2.4}$$

Integrating the product of the absorption and scattering term over x and normalizing over the enhancement factor of an ideal free-standing graphene, the enhancement factor is calculated:

$$F = \frac{1}{F_{fs}} \int_0^{d_2} \|F_{ab}F_{sc}\|^2 \, dx. \tag{5.2.5}$$

6. References

[1] A.K. Geim, K.S. Novoselov, The rise of graphene, Nat. Mater. 6 (2007) 183–191.

[2] R. Muñoz, C. Gómez-Aleixandre, Review of CVD Synthesis of Graphene, Chem. Vap. Depos. 19 (2013) 297–322.

[3] G. Yazdi, T. Iakimov, R. Yakimova, Epitaxial Graphene on SiC: A Review of Growth and Characterization, Crystals. 6 (2016) 53.

[4] A.C. Ferrari, F. Bonaccorso, V. Fal'ko, K.S. Novoselov, S. Roche, P. Bøggild, Science and technology roadmap for graphene, related two-dimensional crystals, and hybrid systems, Nanoscale. 7 (2015) 4598–4810.

[5] C. Mattevi, H. Kim, M. Chhowalla, A review of chemical vapour deposition of graphene on copper, J. Mater. Chem. 21 (2011) 3324–3334.

[6] L. Baraton, Z.B. He, C.S. Lee, C.S. Cojocaru, M. Châtelet, J.-L. Maurice, Y.H. Lee, D. Pribat, On the mechanisms of precipitation of graphene on nickel thin films, EPL. 96 (2011) 46003.

[7] L. Huang, Q.H. Chang, G.L. Guo, Y. Liu, Y.Q. Xie, T. Wang, B. Ling, H.F. Yang, Synthesis of high-quality graphene films on nickel foils by rapid thermal chemical vapor deposition, Carbon N. Y. 50 (2012) 551–556.

[8] H. Ago, Y. Ito, N. Mizuta, K. Yoshida, B. Hu, C.M. Orofeo, M. Tsuji, K.-I. Ikeda, S. Mizuno, Epitaxial chemical vapor deposition growth of single-layer graphene over cobalt film crystallized on sapphire, ACS Nano. 4 (2010) 7407–7414.

[9] M. Losurdo, M.M. Giangregorio, P. Capezzuto, G. Bruno, Graphene CVD growth on copper and nickel: role of hydrogen in kinetics and structure, Phys. Chem. Chem. Phys. 13 (2011) 20836–20843.

[10] G. Amato, F. Beccaria, F. Celegato, Growth of strained, but stable, graphene on Co, Thin Solid Films. 638 (2017) 324–331.

[11] M. Hasebe, H. Ohtani, T. Nishizawa, Effect of magnetic transition on solubility of carbon in bcc Fe and fee Co-Ni alloys, MTA. 16 (1985) 913–921.

[12] J. Ye, C.V. Thompson, Anisotropic edge retraction and hole growth during solid-state dewetting of single crystal nickel thin films, Acta Mater. 59 (2011) 582–589.

[13] D.J. Srolovitz, S.A. Safran, Capillary instabilities in thin films. I. Energetics, J. Appl. Phys. 60 (1986) 247–254.

[14] P.J. Wessely, F. Wessely, E. Birinci, K. Beckmann, B. Riedinger, U. Schwalke, Silicon-CMOS compatible in-situ CCVD grown graphene transistors with ultra-high on/off-current ratio, Physica E. 44 (2012) 1132–1135.

[15] C. Si, Z. Sun, F. Liu, Strain engineering of graphene: a review, Nanoscale. 8 (2016) 3207–3217.

[16] Z.H. Ni, T. Yu, Y.H. Lu, Y.Y. Wang, Y.P. Feng, Z.X. Shen, Uniaxial strain on graphene: Raman spectroscopy study and band-gap opening, ACS Nano. 2 (2008) 2301–2305.

[17] L.M. Malard, M.A. Pimenta, G. Dresselhaus, M.S. Dresselhaus, Raman spectroscopy in graphene, Phys. Rep. 473 (2009) 51–87.

[18] L. Croin, E. Vittone, G. Amato, Low-temperature rapid thermal CVD of nanocrystalline graphene on Cu thin films: Low-temperature rapid thermal CVD of nanocrystalline graphene on Cu, Phys. Status Solidi . 251 (2014) 2515–2520.

[19] G. Amato, G. Milano, U. Vignolo, E. Vittone, Kinetics of defect formation in chemically vapor deposited (CVD) graphene during laser irradiation: The case of Raman investigation, Nano Res. 8 (2015) 3972–3981.

[20] S.D. Costa, A. Righi, C. Fantini, Y. Hao, C. Magnuson, L. Colombo, R.S. Ruoff, M.A. Pimenta, Resonant Raman spectroscopy of graphene grown on copper substrates, Solid State Commun. 152 (2012) 1317–1320.

[21] W.X. Wang, S.H. Liang, T. Yu, D.H. Li, Y.B. Li, X.F. Han, The study of interaction between graphene and metals by Raman spectroscopy, J. Appl. Phys. 109 (2011) 07C501.

[22] D. Yoon, H. Moon, Y.-W. Son, J.S. Choi, B.H. Park, Y.H. Cha, Y.D. Kim, H. Cheong, Interference effect on Raman spectrum of graphene on SiO 2 / Si, Phys. Rev. B Condens. Matter. 80 (2009) 125422–125428.

[23] A.C. Ferrari, D.M. Basko, Raman spectroscopy as a versatile tool for studying the properties of graphene, Nat. Nanotechnol. 8 (2013) 235–246.

[24] P. Lecaruyer, E. Maillart, M. Canva, J. Rolland, Generalization of the Rouard method to an absorbing thin-film stack and application to surface plasmon resonance, Appl. Opt. 45 (2006) 8419.

[25] A.C. Ferrari, J.C. Meyer, V. Scardaci, C. Casiraghi, M. Lazzeri, F. Mauri, S. Piscanec, D. Jiang, K.S. Novoselov, S. Roth, A.K. Geim, Raman spectrum of graphene and graphene layers, Phys. Rev. Lett. 97 (2006) 187401.

[26] D.R. Lenski, M.S. Fuhrer, Raman and optical characterization of multilayer turbostratic graphene grown via chemical vapor deposition, J. Appl. Phys. 110 (2011) 013720.

[27] A. Das, S. Pisana, B. Chakraborty, S. Piscanec, S.K. Saha, U.V. Waghmare, K.S. Novoselov, H.R. Krishnamurthy, A.K. Geim, A.C. Ferrari, A.K. Sood, Monitoring dopants by Raman scattering in an electrochemically top-gated graphene transistor, Nat. Nanotechnol. 3 (2008) 210–215.

[28] D. Yoon, Y.-W. Son, H. Cheong, Strain-dependent splitting of the double-resonance Raman scattering band in graphene, Phys. Rev. Lett. 106 (2011) 155502.

[29] C. Mattevi, H. Kim, M. Chhowalla, A review of chemical vapour deposition of graphene on copper, J. Mater. Chem. 21 (2011) 3324–3334.

[30] P.R. Shaina, L. George, V. Yadav, M. Jaiswal, Estimating the thermal expansion coefficient of graphene: the role of graphene-substrate interactions, J. Phys. Condens. Matter. 28 (2016) 085301.

[31] D. Yoon, Y.-W. Son, H. Cheong, Negative thermal expansion coefficient of graphene measured by Raman spectroscopy, Nano Lett. 11 (2011) 3227–3231.

[32] D.R. Lide (*ed.*), *CRC Handbook of Chemistry and Physics, 84th Edition*. CRC Press. Boca Raton, Florida, 2003; Section 12, Properties of Solids; Thermal and Physical Properties of Pure Metals

[33] Amato, G. High Temperature Growth of Graphene from Cobalt Volume: Effect on Structural Properties. *Materials* **2018**, *11*, 257

[34] E.D. Palik, Handbook of optical constants of solids, Academic Press, 1998.